2007

Change of Multifractal Thermal Characteristics in the Western Philippine Sea Upper Layer during Internal Wave-Soliton Propagation

Chu, Peter C.; Hsieh, Chung-Ping

Chu, P.C. and C. P. Hsieh, 2007: Change of Multifractal Thermal Characteristics in the Western Philippine Sea Upper Layer during Internal Wave-Soliton Propagation (paper download). Journal of Oceanography, Oceanographic Society of Japan, 63, 927-939.
https://hdl.handle.net/10945/36146

Journal of Oceanography, Vol. 63, pp. 927 to 939, 2007

Change of Multifractal Thermal Characteristics in the Western Philippine Sea Upper Layer during Internal Wave-Soliton Propagation

PETER C. CHU* and CHUNG-PING HSIEH

Naval Ocean Analysis and Prediction Laboratory, Naval Postgraduate School, Monterey, CA 93940, U.S.A.

(Received 8 November 2006; in revised form 2 March 2007; accepted 7 June 2007)

The upper layer (above 140 m depth) temperature in the western Philippine Sea near Taiwan was sampled using a coastal monitoring buoy (CMB) with 15 attached thermistors during July 28–August 7, 2005. The data were collected every 10 min at 1, 3, 5, 10, 15, and 20 m using the CMB sensors, and every 15 sec at 15 different depths between 25 m and 140 m. Internal waves and solitons were identified from the time-depth plot of the temperature field. Without the internal waves and solitons, the power spectra, structure functions, and singular measures (representing the intermittency) of temperature field satisfy the power law with multi-scale characteristics at all depths. The internal waves do not change the basic characteristics of the multifractal structure. However, the internal solitons change the power exponent of the power spectra drastically, especially in the low wave number domain; they also break down the power law of the structure function and increase the intermittency parameter. The physical mechanisms causing these different effects need to be explored further.

Keywords:
· High-order structure function,
· intermittency,
· internal wave,
· internal soliton,
· multifractal analysis,
· power spectrum,
· stationarity,
· singular measure.

1. Introduction

Theories of turbulence as applied to point measurements recorded by buoys drifting in the oceans concern the scaling properties, in a statistical sense, of differenced time series, where the Taylor hypothesis is invoked so that the difference between measurements at some time t and a later time $t + \tau$ acts as a proxy for the difference between measurements made at two points in the fluid separated by length scale l. For a time series $T(x_i)$ with an evenly spaced interval l and a total length L,

$$T_i = T(x_i), \quad x_i = il, \quad i = 0,1,...,\Lambda, \quad L = \Lambda l,$$

an increment series

$$|\Delta T(x_i, rl)| = |T(x_{i+r}) - T(x_i)|, \quad i = 0,1,...,\Lambda - r \qquad (1)$$

can be constructed with respect to the increment rl (r is an integer).

Studies of scaling in upper ocean turbulence have focused on the power spectra and the structure functions (see e.g. Chu, 2004). The q-th order structure function is defined by

$$S(r,q) \equiv \left\langle |\Delta T(x, rl)|^q \right\rangle = \frac{1}{\Lambda - r} \sum_{i=0}^{\Lambda - r} |\Delta T(x_i, rl)|^q. \qquad (2)$$

Here, r is inversely proportional to the wavenumber l,

$$r \propto \frac{1}{l}.$$

Obviously, for small r, $\Delta T(x_i, rl)$ represents the small-scale fluctuations (usually turbulence). The first-order structure function $S(r, 1)$ was initially introduced to study small-scale turbulence where it appeared to be an effective tool in linking turbulence physics with statistics. The scale-invariance of the variable T is represented by

$$|\Delta T(x_i, l)| = r^{-H} |\Delta T(x_i, rl)|, \qquad (3)$$

where H is the scaling exponent, called the Hurst exponent. In 1941, Kolmogorov suggested that the velocity

* Corresponding author. E-mail: pcchu@nps.edu

increment in high-Reynolds number turbulent flows should scale with the mean (time-averaged) energy dissipation and the separation length scale. The Hurst exponent H is equal to 1/3. For the q-th order structural function, simple self-similarity implies

$$\left\langle \left|\Delta T(x_i, l)\right|^q \right\rangle = r^{-qH} \left\langle \left|\Delta T(x_i, rl)\right|^q \right\rangle. \quad (4)$$

Multifractal behavior may be generalized from (4) into

$$\left\langle \left|\Delta T(x_i, l)\right|^q \right\rangle = r^{-\zeta(q)} \left\langle \left|\Delta T(x_i, rl)\right|^q \right\rangle. \quad (5)$$

In other words, simple self-similarity may be described with a single scaling exponent H, while multifractal scale-invariance requires a spectrum of scaling exponents with

$$\zeta(q) \neq qH.$$

In the case of multifractality, $\langle|\Delta T(x_i, l)|^q\rangle$ does not scale in the same way as $\langle|\Delta T(x_i, l)|\rangle^q$, which would be the case for simple self-similarity. Given the above consideration, the scaling behavior of the structure function may be expressed by

$$S(r, q) \sim r^{\zeta(q)}, \quad (6)$$

where the spectral exponent $\zeta(q)$ is independent of the energy input mechanism. The ensemble of $\Delta T(x_i, rl)$ is invariant under translations and rotations for length scale smaller than the energy input scale.

The multifractal scaling characteristics of the upper layer thermal structure were found for the southwestern Greenland Sea, Iceland Sea, and Norwegian Sea (GIN Sea) using high-resolution, digital thermistor chain data from the surface to 140 m deep. A linear dependence of $\mathrm{Log}_2[S(r, q)]$ on $\mathrm{Log}_2(r)$ is found, with different q-values ranging from 0.5 to 4.0 (Chu, 2004).

Does multifractal scaling occur in other seas, such as the western Philippine Sea (WPS) near Taiwan (Fig. 1)? This is the region where the Philippines Current flows northward from just north of Mindanao (the southernmost of the main island groups of the Philippines) at around (10°N, 128°E) to Taiwan, where it continues as the Kuroshio—the most evident western boundary current in the North Pacific Ocean. After it becomes the Kuroshio, it makes a slight excursion into the South China Sea through the Luzon Strait, continues northward, and is fed from the North Equatorial Current, from which it continues to entrain water along its path. This current system has various stages of modification that transport warm water to the North Pacific. The import and modification

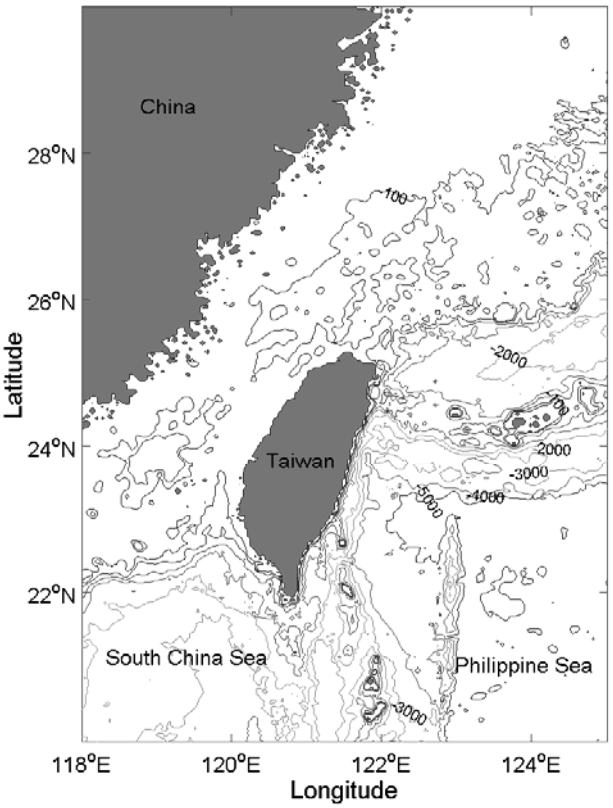

Fig. 1. Topography of the western Philippine Sea and surrounding areas.

of water masses means that a large number of regional water types can be encountered. Eddy activity is often observed in WPS near Taiwan. For example, a large warm eddy lies east of the Luzon Strait, which is a seemingly permanent feature (Nitani, 1972; Chu and Li, 2000; Chu and Fan, 2001). Although the WPS is the only significant source of open-ocean water to the South China Sea, the hydrographic and chemical properties of the waters on both side of the Luzon Strait are quite different (Nitani, 1972). When the Kuroshio branches out near the southern tip of Taiwan, part of the current intrudes into the South China Sea through the Luzon Strait. The internal tides and internal waves are probably generated by the shallow ridges in the Luzon Strait (Liu *et al*., 1998). During the Asian Seas International Acoustics Experiment for the South China Sea, a moored array of current, temperature, conductivity, and pressure sensors was deployed across the Chinese continental shelf and slope. By far the most dominant oceanographic signal was in fact the highly nonlinear internal waves (or solitons), which were generated near the Batan Islands in the Luzon Strait and propagated 485 km across deep water to the observation region (i.e., northern South China Sea) (Ramp *et al*., 2004).

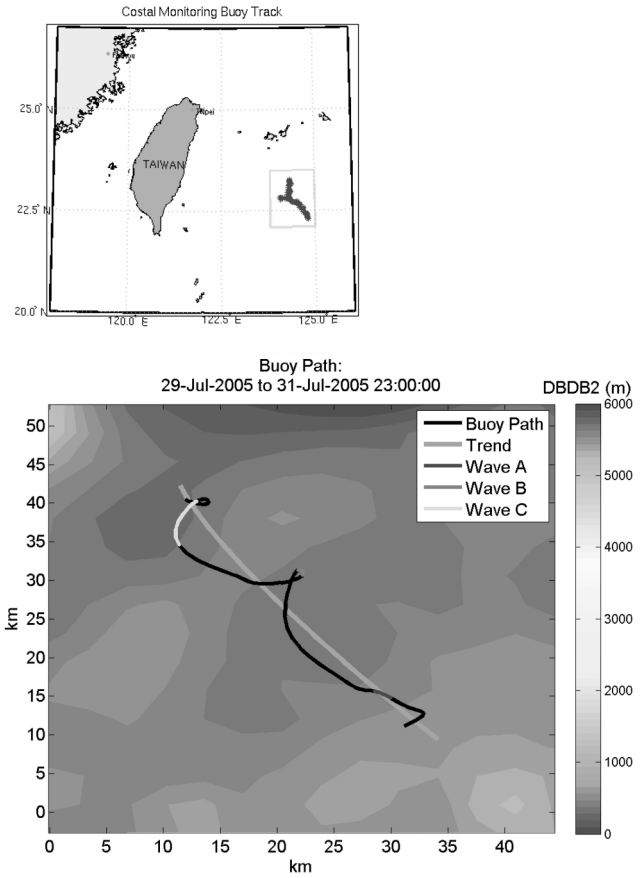

Fig. 2. Track of CMB (from July 28 to August 7, 2005) deployed by the Naval Oceanographic Office.

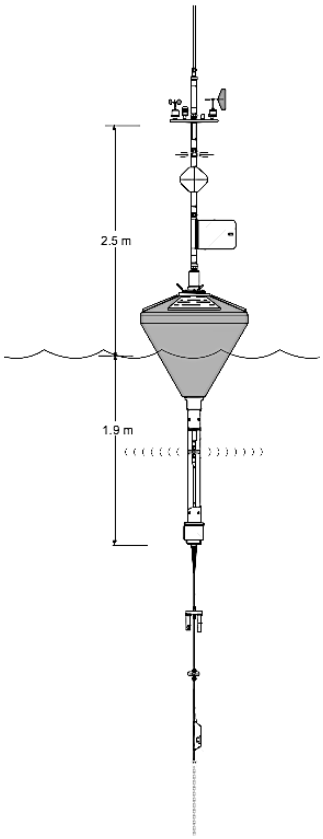

Fig. 3. Coastal Monitoring Buoy used in the WPS survey. Fifteen thermistors are attached to a wire rope extending from the code of CMB (20 m deep) to 140 m with high frequency sampling rate (every 15 sec).

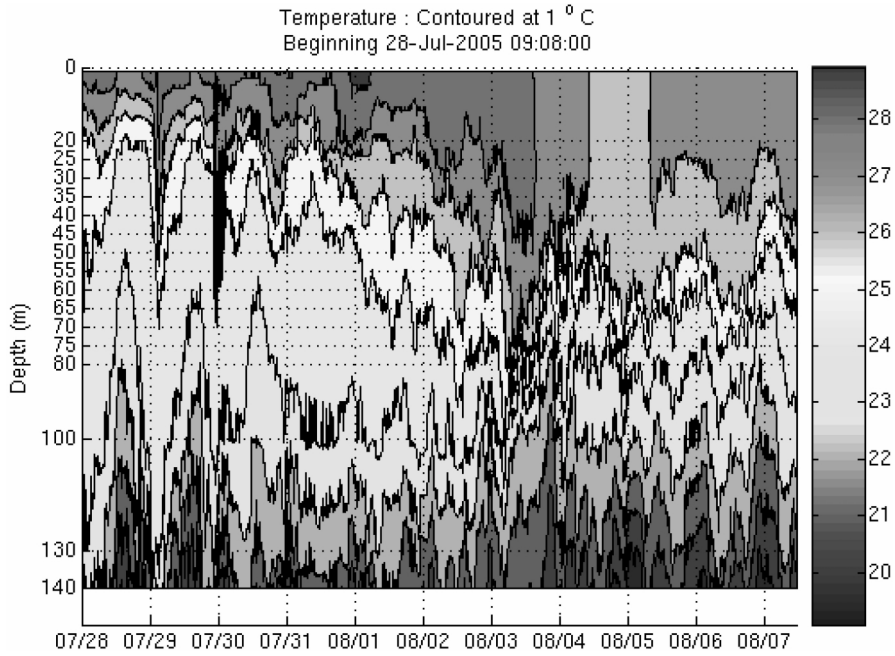

Fig. 4. Time-depth cross section of temperature obtained from the CMB data collected along the track shown in Fig. 2.

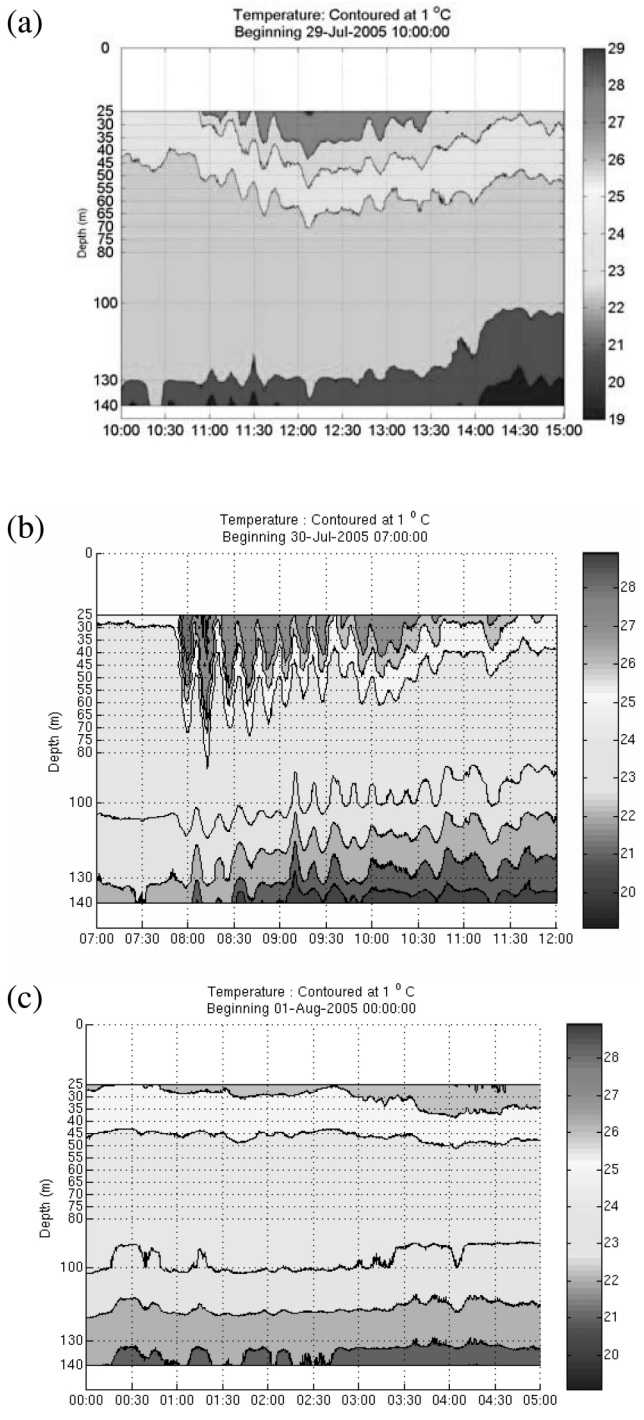

Fig. 5. Time-depth cross section of temperature on (a) 1000–1500 GMT July 29 (IW-turbulence), (b) 0700–1200 GMT July 30 (IS-turbulence), and (c) 0000–0500 GMT August 1 (turbulence-dominated) obtained from the CMB data collected along the track shown in Fig. 2.

Since highly nonlinear internal waves (or solitons) often occur in the Kuroshio region near Taiwan, one may ask whether multifractal scaling exists in the upper layer thermal field? What are the effects of internal wave and soliton propagation? To obtain turbulence and internal wave/soliton signals, we need high temporal resolution data of relatively long duration. Recently, a coastal monitoring buoy (CMB) with 15 thermistors attached at various depths was deployed by the U.S. Naval Oceanographic Office in WPS (Fig. 2) during July 28–August 7, 2005. The sampling rate of the thermistors is one record every 15 s. These observations provide useful data for investigating the multifractal feature of the upper layer of WPS in the presence of internal waves and solitons.

2. Data Description

The original design of CMB is to collect the data every 10 min near the air-ocean interface (Chu and Hsieh, 2007). Surface winds, air temperature, and air pressure are measured above the ocean surface. Temperature is observed at 1, 3, 5, 10, 15, and 20 m below the ocean surface. During the observation period (July 28–August 7, 2005) the CMB traveled 229.14 km along the track (Fig. 2), with an average speed of 3.82 m per 15 sec. The surface winds are weak (around 4 m/s) and the surface air temperature is close to the water temperature at 1 m depth (implying weak buoyancy flux across the air-ocean interface). Weak surface winds and buoyancy fluxes created shallow surface mixed layer.

Fifteen thermistors are attached to a wire rope extending from the code of CMB (20 m deep) to 140 m with high frequency sampling rate (every 15 sec) (Fig. 3). The time-depth cross section of temperature along the CMB track shows multi-scale variability with a highly irregular nature (Fig. 4). The surface mixed layer is very thin (depth around 5 m) on July 28 with temperature about 28.5°C. Below the surface mixed layer, two thermoclines appear, with the first thermocline at a depth of 50 m. The vertical gradient in the first thermocline is around 0.1 °C/m. A relatively uniform sublayer (24°C) exists below the first thermocline from 50 to 130 m. Below the uniform sublayer there is a second thermocline with a vertical temperature gradient around 0.04°C/m. As time passes, the surface mixed layer deepens and the first thermocline descends. These processes contain small scale fluctuations. The surface mixed layer reaches 70 m on August 5, when evident cooling occurs as the mixed layer temperature reduces to 25.5°C. At the same time, the two thermoclines merge to a single themocline with a vertical gradient of 0.06°C/m.

3. Temperature Anomaly

During the temperature sampling by CMB thermistors (Fig. 4), temperature anomaly in the upper

layer can be calculated by

$$T'(t,z) = T(t,z) - \overline{T}(z), \tag{7}$$

which is the deviation of the observed temperature from the time-mean temperature. Without salinity data, the isopycnal displacement is calculated by (Desaubles and Gregg, 1981)

$$\eta(t,z) = -\frac{T'(t,z)}{d\overline{T} / dz}, \tag{8}$$

which fluctuates with various amplitudes (A_η). Three types can be identified according to the magnitude of A_η: (a) turbulence-dominated type ($A_\eta \leq 5$ m); (b) internal wave (IW)-turbulence type (5 m < $A_\eta \leq 30$ m); and (c) internal soliton (IS)-turbulence type ($A_\eta > 30$ m). During the entire observational period (28 July to 7 August 2005), the IS-turbulence type occurs only on 0700–1200 GMT July 30, 2005 (Fig. 4). Two 5-hr periods before and after the occurrence of the IS-turbulence type are chosen for comparison (Fig. 5): 1000–1500 GMT July 29, 2005 (IW-turbulence type), and 0000–0500 GMT August 1 (turbulence-dominated type). During the remaining six days (0500 GMT August 1 to 7 August 2005), the IW-turbulence type occurs more often than the turbulence-dominated type.

Since the upper ocean is usually turbulent due to mixing, the turbulence-dominated, IW-turbulence, and IS-turbulence types are regarded an absence of internal waves, the existence of internal waves, and the existence of internal solitons. In other words, generation, growth, propagation, and dissipation are the factors controlling the alternative occurrence of IW-turbulence, IS-turbulence and turbulence-dominated types. The generation of internal waves is most often attributed in some way to tidal flow across abrupt topography (Ramp *et al*., 2004). In the absence of *in situ* information at the generation site to describe the dynamics, this manuscript focuses mainly on describing the change of the multifractal thermal structure with the propagation of internal waves and internal solitons.

For the IW-turbulence type (1000–1500 GMT July 29, 2005, Fig. 6(a)), the maximum temperature fluctuation decreases with depth from ±1.6°C at the surface to ±0.4°C at 100 m depth and then increases with depth to ±1°C at 140 m. For the IS-turbulence type (0700–1200 GMT July 30, 2005, Fig. 6(b)), the maximum temperature fluctuation increases with depth from ±1.8°C at the surface to ±2.9°C at 60 m depth, then decreases with depth to ±0.8°C at 100 m, and finally increases with depth to ±2.1°C at 140 m. For the dominant-turbulence type (0000–0500 GMT August 1, Fig. 6(c)), the maximum temperature fluctuation decreases with depth from ±1.3°C at the surface to ±0°C at 60–65 m depth, and then increases with depth to ±0.9°C at 140 m.

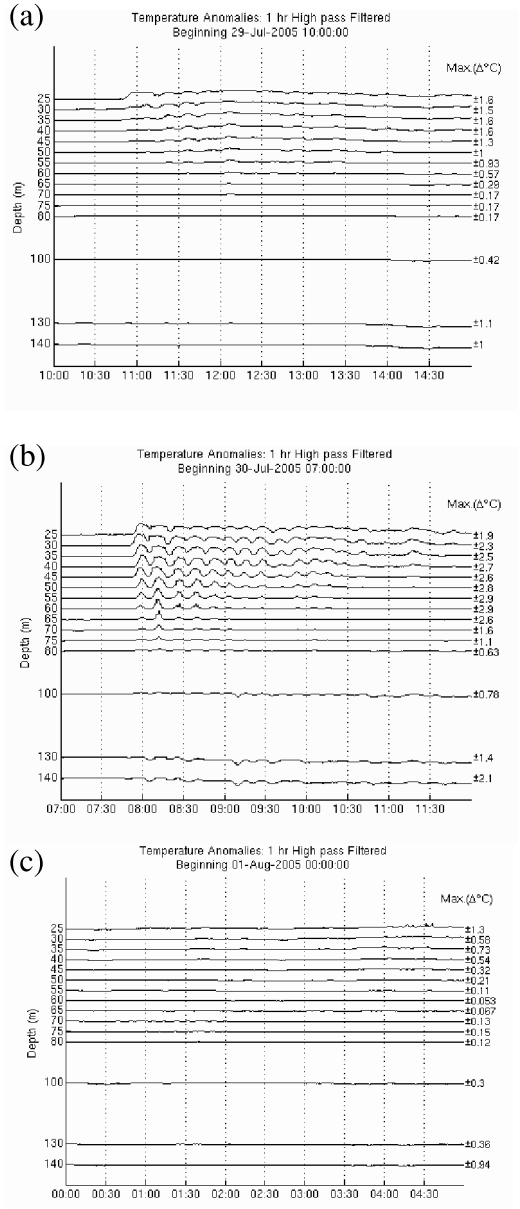

Fig. 6. Temporal variation of temperature anomaly at the thermistor depth on (a) 1000–1500 GMT July 29 (IW-turbulence), (b) 0700–1200 GMT July 30 (IS-turbulence), and (c) 0000–0500 GMT August 1 (turbulence-dominated), 2005.

The observed temperature profile oscillates during the IW-turbulence type (1000–1500 GMT July 29, Fig. 7(a)) and IS-turbulence type (0700–1200 GMT July 30, Fig. 7(b)), but not during the turbulence-dominated type (0000–0500 GMT, August 1). The oscillation is evident

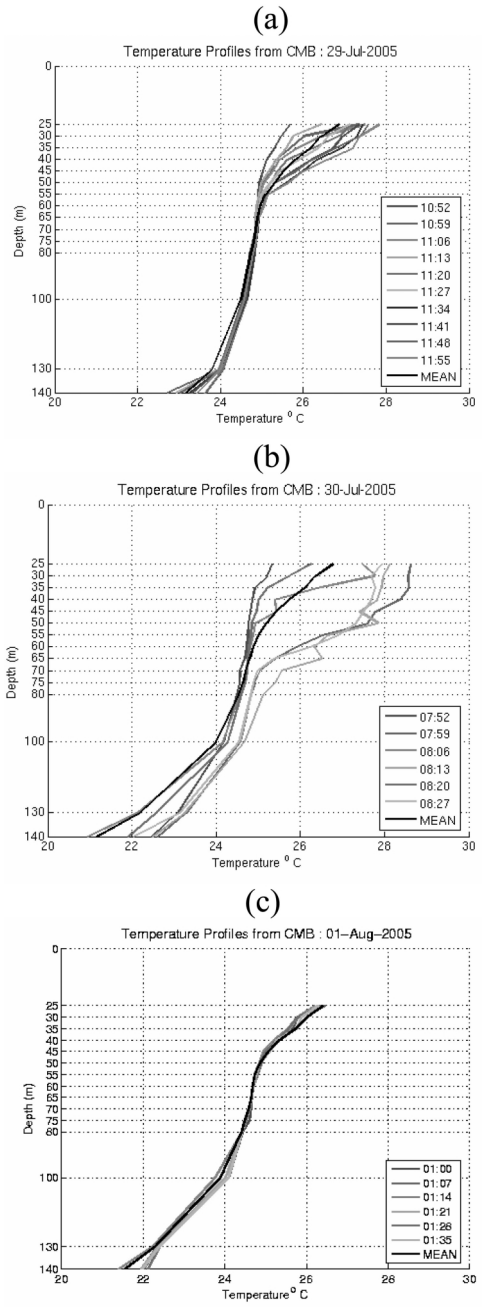

Fig. 7. Temporally varying temperature profiles observed from CMB thermistors on (a) 1000–1500 GMT July 29 (IW-turbulence), (b) 0700–1200 GMT July 30 (IS-turbulence), and (c) 0000–0500 GMT August 1 (turbulence-dominated), 2005. Oscillation of the temperature profiles is found in (a) and (b) with period around 14 min, but not in (c). The amplitude of the oscillation is much larger in (b) than in (a).

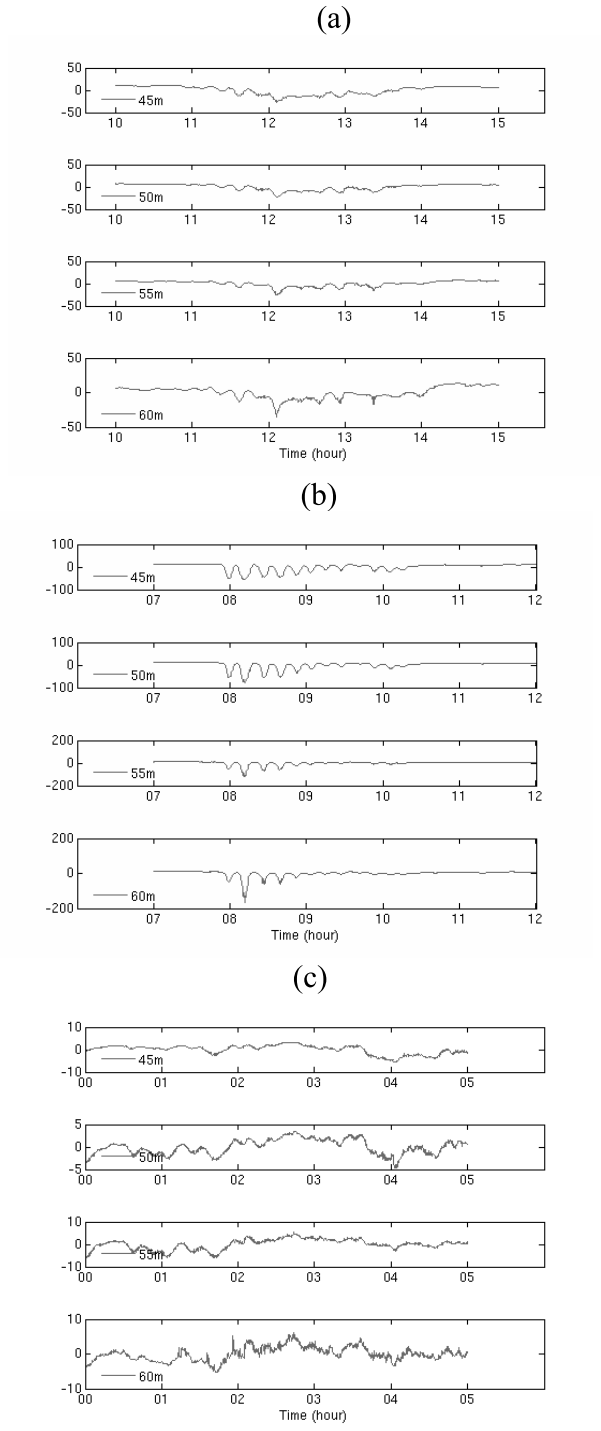

Fig. 8. Isopycnal displacements measured by thermistors at 45 m, 50 m, 55 m, and 60 m depths on (a) 1000–1500 GMT July 29 (IW-turbulence), (b) 0700–1200 GMT July 30 (IS-turbulence), and (c) 0000–0500 GMT August 1 (turbulence-dominated), 2005. The isopycnal displacement is strongest in (b) with a maximum value of around 160 m at 80 m depth, and in (b) and weakest in (c) with maximum value less than 5 m.

in the upper layer above 50 m in the IW-turbulence type and above 80 m in the IS-turbulence type. This may be related to the different descent of the first thermocline to 80 m for the IS-turbulence type and 50 m for the IW-

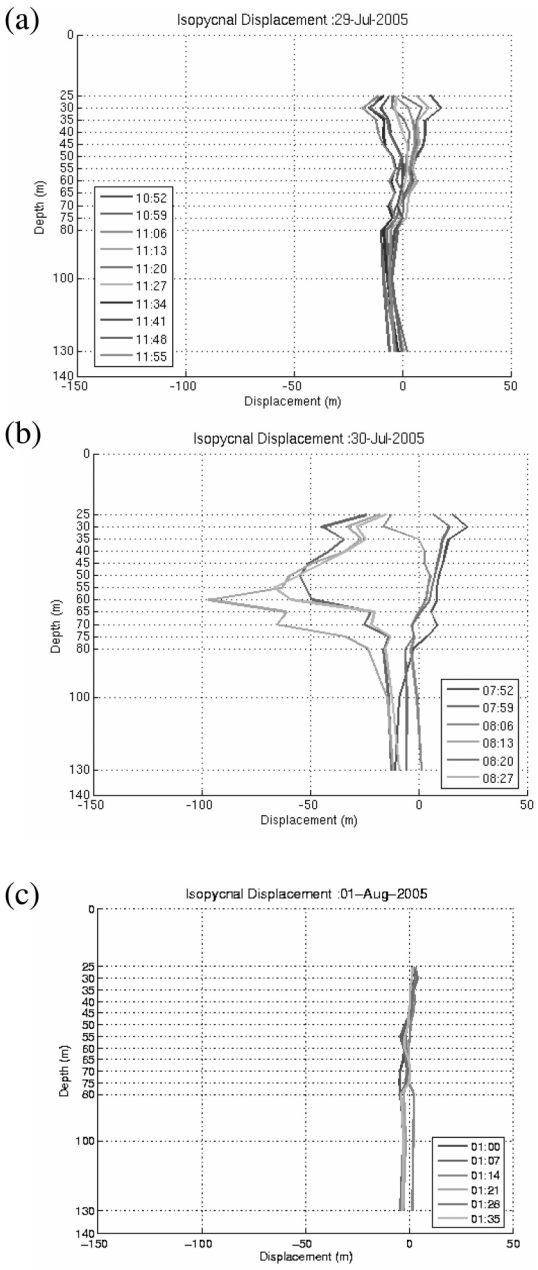

Fig. 9. Temporally varying isopycnal displacement identified from CMB thermistors on (a) 1000–1500 GMT July 29 (IW-turbulence), (b) 0700–1200 GMT July 30 (IS-turbulence), and (c) 0000–0500 GMT August 1 (turbulence-dominated), 2005. Oscillation of the isopycnal displacement is found in (a) and (b) with period around 14 min, but not in (c). The amplitude of the oscillation is much larger in (b) than in (a).

turbulence type (Fig. 4). Moreover, the amplitude of the oscillation is much larger in the IS-turbulence type (maximum amplitude around 4°C) than the IW-turbulence type (maximum amplitude around 2°C). For the IS-turbulence type (Fig. 7(b)), the temperature profiles measured with the 15 thermistors are found to oscillate with period 7 min from 0752 to 0827 GMT July 30, 2005. The black curve in Fig. 7(b) is the mean temperature profile over the entire CMB track (i.e., $\overline{T}(z)$). The temperature profile on 0752 GMT (blue curve) represents a cool upper layer with temperature 25.3°C at 25 m depth (minimum among the five profiles). Seven minutes later (0757 GMT), the profile (green curve) represents a warm upper layer with temperature 28.7°C at 25 m depth (maximum among the five profiles). Fourteen minutes later, the profile (red curve) shifts to the cool upper layer.

4. Isopycnal Displacement

The isopycnal displacement $\eta(t, z)$ at four different depths (40 m, 45 m, 55 m, and 60 m) is used for illustration. During the IW-turbulence type (1000–1500 GMT July 29, Fig. 8(a)), the isopycnal displacement oscillates with time and has maximum downwelling (20 m) at all four depths at 1200 GMT July 29, 2005 (Fig. 8(a)). For the IS-turbulence type (0700–1200 GMT July 30, Fig. 8(b)), the amplitude of isopycnal displacement $\eta(t, z)$ is around 50 m at 45 and 50 m depths, increasing to near 100 m at 60 m depth with frequency around 4 CPH. For the turbulence-dominated type (0000–0500 GMT August 1, Fig. 8(c)), the isopycnal displacement is very small with maximum amplitude around 4–6 m.

Similar to the temperature profile, the isopycnal displacement profile oscillates in the IW-turbulence type (1000–1500 GMT July 29, Fig. 9(a)) and IS-turbulence type (0700–1200 GMT July 30, Fig. 9(b)), but not in the turbulence-dominated type (0000–0500 GMT, August 1, Fig. 9(c)). The oscillation is evident in the upper layer above 50 m in the IW-turbulence type and above 80 m in the IS-turbulence type. The amplitude of the oscillation is much larger in the IS-turbulence type (maximum amplitude around 100 m) than the IW-turbulence type (maximum amplitude around 20 m).

Figure 9(b) shows time evolution of the isopycnal displacement profiles with 7 min apart from 0752 to 0827 GMT July 30, 2005. On 0752 GMT (blue curve), the profile represents upward displacement with a maximum value of 20 m at 30 m depth. Seven minutes later (0757 GMT), the profile (green curve) represents downward displacement with a maximum value of –100 m at 60 m depth. Fourteen minutes later, the profile (red curve) represents weak displacement.

5. Power Spectra

The energy spectra of the isopycnal displacement (ϕ_η) is related to the temperature variance spectra (ϕ_T) by

$$\phi_\eta = \left\langle \frac{d\overline{T}}{dz} \right\rangle^{-2} \phi_T . \qquad (9)$$

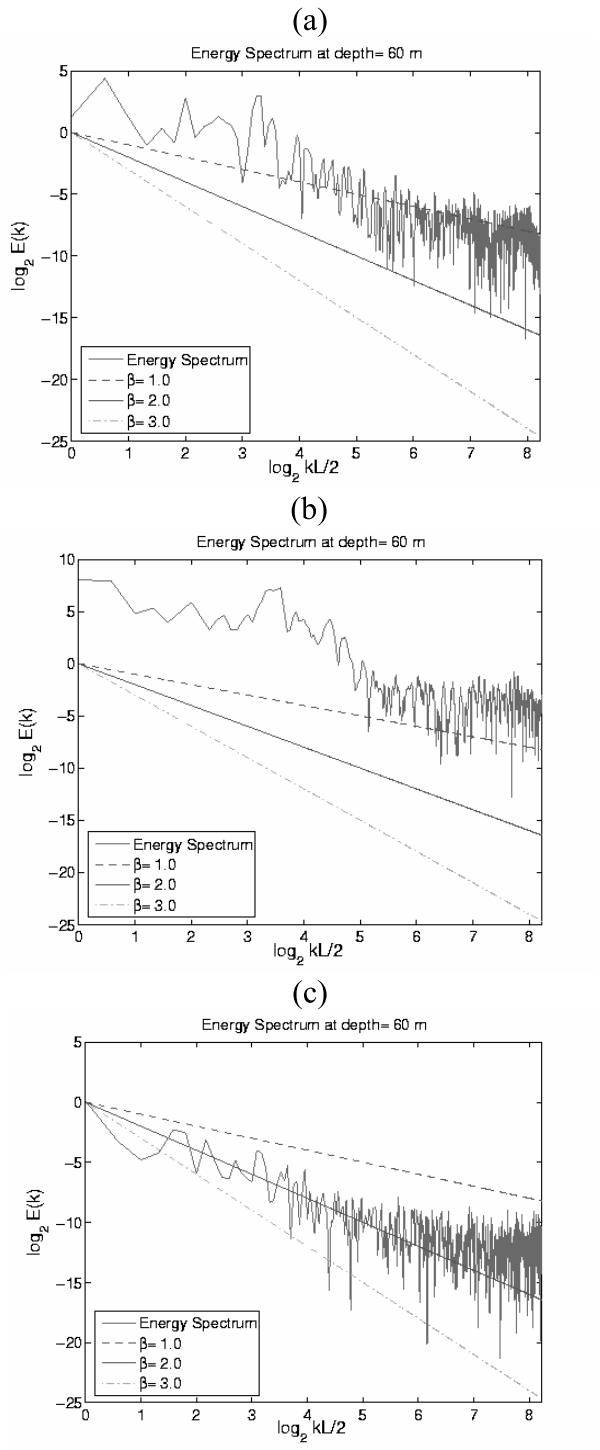

Fig. 10. Power spectra of temperature at 60 m deep on (a) 1000–1500 GMT July 29 (IW-turbulence), (b) 0700–1200 GMT July 30 (IS-turbulence), and (c) 0000–0500 GMT August 1 (turbulence-dominated), 2005.

Since the statistical features of isopycnal displacement and temperature are related to each other, we only investigate the difference in the statistical structure of the temperature field in IW-turbulence, IS-turbulence, and turbulence-dominated types.

Determination of stationarity is the first step in understanding the inherent thermal variability and statistical properties identified from this high-resolution temperature data with multi-layer structures. As mentioned in Section 2, the CMB collects data every 15 sec and travels with an average speed of 3.82 m per 15 sec. For a given depth, the temperature data is a function of the horizontal coordinates, x, $T_i = T(x_i)$, $x_i = il$, and $l = 3.82$ m. For each of the three types (IW-turbulence, IS-turbulence, and turbulence-dominated), there are 1,200 temperature profiles ($\Lambda = 1{,}200$).

Spectral analyses of temperature field,

$$E_j = E\left(k_j\right), \quad k_j = j/L, \quad j = 1,2,...,\Lambda/2, \quad L = \Lambda l \qquad (10)$$

at all depths for each type are conducted, but for the sake of brevity and to elucidate the important points, only spectra at 60 m depth are shown in Fig. 10. A Bartlett window was used to taper the ends of each series before calculating the power spectra to reduce the spectral leakage in the wavenumber domain.

For a scaling process, one expects power law behavior (Chu *et al.*, 2002; Chu, 2004),

$$E(k) \propto k^{-\beta}, \qquad (11)$$

over a large range of wavenumber k. The spectral exponent β contains information about the degree of stationarity of the data. If $\beta < 1$, the field is stationary; if $1 < \beta < 3$, the field contains a nonstationary signal with stationary increments and, in particular, the small-scale gradient field is stationary; if $\beta > 3$, the field is nonstationary with nonstationary increments.

The power spectra for the IW-turbulence (Fig. 10(a)) and turbulence-dominated type (Fig. 10(c)) have similar multi-scaling characteristics with almost the same spectral exponent β: around 0.4 (stationary) for low wavenumbers ($\log_2 kL/2 < 4$), and nearly 5/3 (non-stationary with stationary increment) for high wavenumbers ($\log_2 kL/2 > 4$). However, the power $E(k)$ is much larger for the IW-turbulence type than the turbulence-dominated type, which implies that the energy is distributed over all wavenumbers during the internal wave propagation.

The spectrum of the IS-turbulence type (Fig. 10(b)) is quite different from the two other spectra, especially in the spectral exponent β: around 0.4 (stationary) for low wavenumbers ($\log_2 kL/2 < 3.5$), nearly 4.2 (non-stationary with non-stationary increment) for mid-range

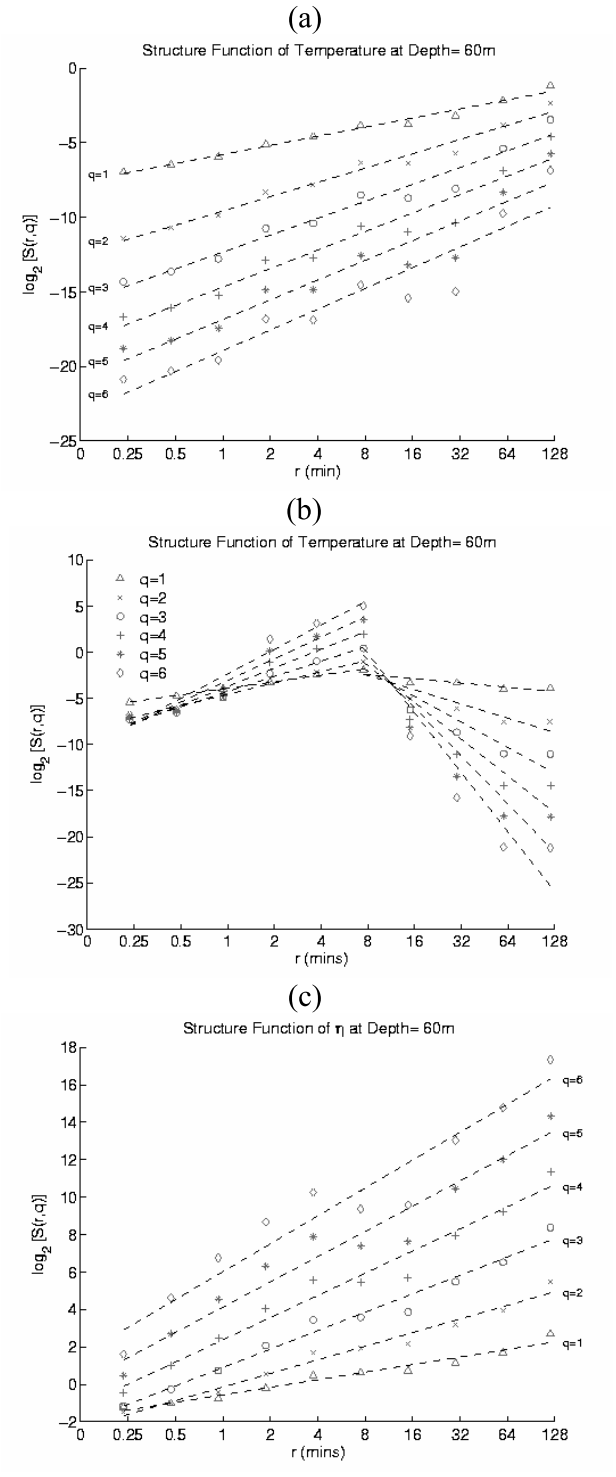

Fig. 11. Statistical structure functions of temperature at 60 m depth on (a) 1000–1500 GMT July 29 (IW-turbulence), (b) 0700–1200 GMT July 30 (IS-turbulence), and (c) 0000–0500 GMT August 1 (turbulence-dominated), 2005.

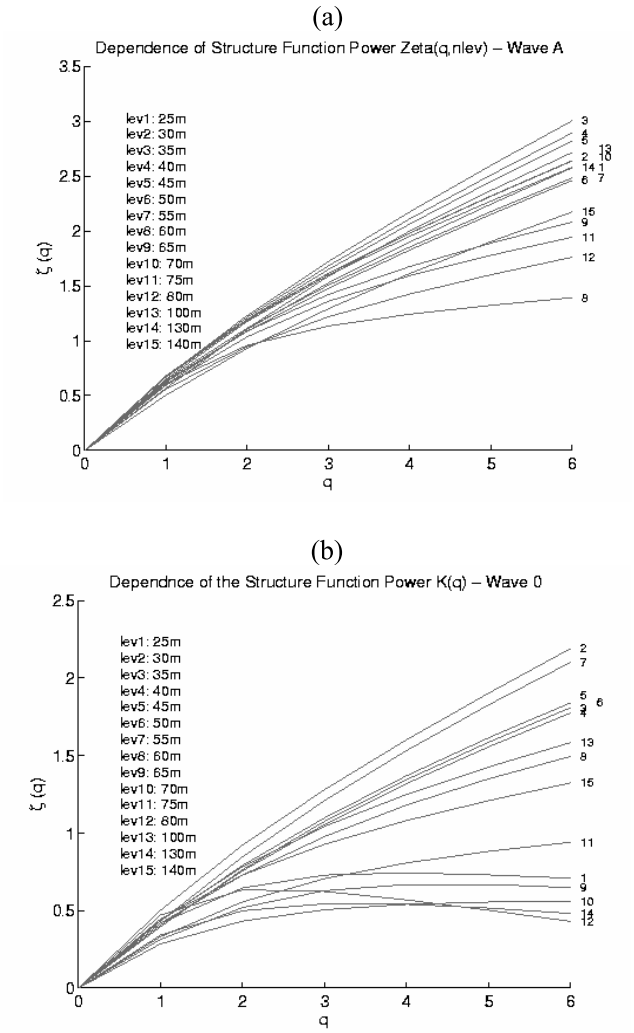

Fig. 12. Dependence of the structure function's power, $\zeta(q)$, on q and depth for (a) 1000–1500 GMT July 29 (IW-turbulence), and (b) 0000–0500 GMT August 1 (turbulence-dominated), 2005.

wavenumbers ($3.5 < \log_2 kL/2 < 6$), approximately 5/3 (non-stationary with stationary increment) for high wavenumbers ($\log_2 kL/2 > 6$).

6. Structure Functions

The structure function (2) is computed for the three types: (a) IW-turbulence (1000–1500 GMT July 29), (b) IS-turbulence (0700–1200 GMT July 30), and (c) turbulence-dominated (0000–0500 GMT August 1) types. A near-linear dependence of $\mathrm{Log}_2[S(r, q)]$ on $\mathrm{Log}_2(r)$ is found with different q-values from 1 to 6 for the IW-turbulence type (Fig. 11(a)) and turbulent-dominated type (Fig. 11(c)), i.e., the structure function $S(r, q)$ satisfies the power law (6) with the exponent $\zeta(q)$ depending only on q. The power of the structure function $\zeta(q)$ increases

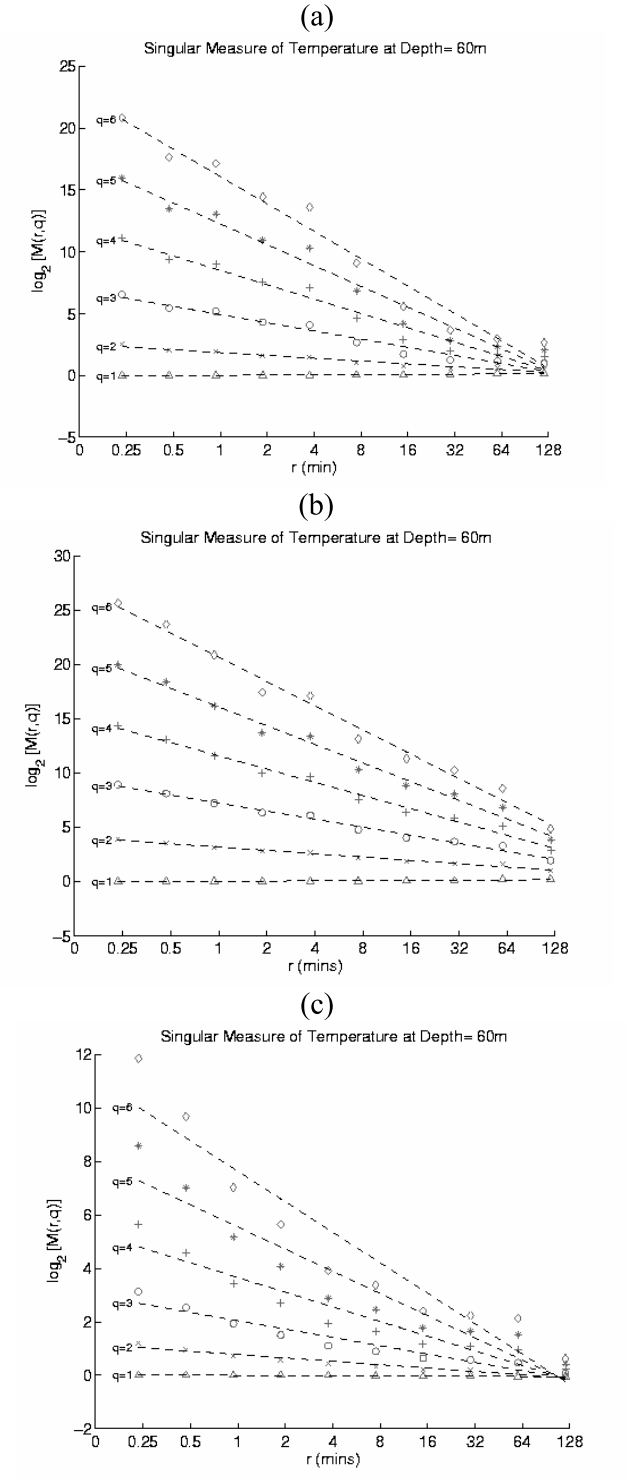

Fig. 13. Singular measures of temperature at 60 m depth on (a) 1000–1500 GMT July 29 (IW-turbulence), (b) 0700–1200 GMT July 30 (IS-turbulence), and (c) 0000–0500 GMT August 1 (turbulence-dominated), 2005.

monotonically and near-linearly with q. However, the structure function $S(r, q)$ for the IS-turbulence type does not satisfy (6) (Fig. 11(b)). The power law is broken approximately at r = 8 min, which is nearly one half period of the IS (with frequency of 4 CPH). This phenomenon occurs at all depths.

Figure 12 shows the dependence of the structure function's power, $\zeta(q)$, on q and depth for (a) 1000–1500 GMT July 29 (IW-turbulence), and (b) 0000–0500 GMT August 1 (turbulence-dominated), 2005. For $q \le 1$, there is not much difference between the two types. The difference becomes evident as q increase. For q = 6, the power $\zeta(q)$ varies from 0.5 to 2.1 for the turbulence-dominated type, but from 1.2 to 3.0 for the IW-turbulence type. This indicates that the internal waves increase the power of the structure function especially at high moments. This may be related to the higher energy in each mode of the IW-turbulence type than the turbulence-dominated type (Figs. 10(a) and (c)).

7. Singular Measures

The normalized small scale absolute gradient

$$\varepsilon(x_i,l)=\frac{|\Delta T(x_i,l)|}{\langle|\Delta T(x_i,l)|\rangle},\quad \langle|\Delta T(x_i,l)|\rangle=\frac{1}{\Lambda}\sum_{i=0}^{\Lambda-1}|\Delta T(x_i,l)|, \quad (12)$$

is used to identify the intermittency (or tendency to periodic halting) of the thermal field. The running average of r normalized values are computed by

$$\varepsilon(x_i,rl)=\frac{1}{r}\sum_{j=i}^{i+r-1}\varepsilon(x_j,l),\quad i=0,1,...,\Lambda-r. \quad (13)$$

The mean of the q-th power of $\varepsilon(x_i, rl)$

$$M(r,q)\equiv\langle\varepsilon(x_i,rl)^q\rangle=\frac{1}{\Lambda-r}\sum_{i=0}^{\Lambda-r}[\varepsilon(x_i,rl)]^q, \quad (14)$$

is defined as the q-th-order singular measure. Obviously, for q = 0,

$$M(r, 0) = 1. \quad (15)$$

For q = 1,

$$M(r,1)\equiv\langle\varepsilon(x_i,rl)\rangle=\frac{1}{\Lambda-r}\sum_{i=0}^{\Lambda-r}[\varepsilon(x_i,rl)]$$
$$=\frac{1}{\Lambda-r}\sum_{i=0}^{\Lambda-r}\left[\frac{1}{r}\sum_{j=i}^{i+r-1}\varepsilon(x_j,l)\right]=1. \quad (16)$$

The singular measures are computed for all depths. For simplicity, $M(r, q)$ of the three types at 60 m deep is given here (Fig. 13). Near-linear dependence of $\mathrm{Log}_2[M(r, q)]$ on $\mathrm{Log}_2(r)$ is found for all the three types with different q-values from 1 to 6. The straight lines with different slopes show that the singular measures with various q for the upper layer temperature in the WPS satisfy the power law

$$M(r,q) \propto r^{-K(q)}, \quad q \geq 0, \tag{17}$$

with the power $K(q)$ varying with q.

It should be noted that for the IS-turbulence type, the power law is broken in the structure function (Fig. 11(b)) but satisfied in the singular measure (Fig. 13(b)). This indicates that the internal solitons destroy the self-similarity in stationary features (structural function) and preserve the self-similarity in intermittent features (singular measure). Such a difference may be caused by the running average of r normalized absolute gradients for the singular measure. Large perturbations caused by IS propagation are smoothed out and the self-similarity feature is preserved.

From Eqs. (15) and (16), we have

$$K(0) = K(1) = 0. \tag{18}$$

Several characteristics are found from Fig. 13: The power $K(q)$ is a convex function

$$\frac{d^2K(q)}{dq^2} > 0, \tag{19}$$

for all q and

$$K(q) < 0 \ \text{ only if } \ 0 < q < 1 \tag{20}$$

which reflects the fact that, in this range, taking a q-th power necessarily reduces the fluctuation of $\varepsilon(r; x_i)$; and otherwise

$$K(q) \geq 0 \ \text{ if } \ q \geq 0. \tag{21}$$

Following Chu (2004), we may define a function

$$C(q) = \frac{K(q)}{q-1}. \tag{22}$$

For $q \to 1$, we use *I'Hospital*'s rule to define a straightforward measure of inhomogeneity in the sense of singular measure

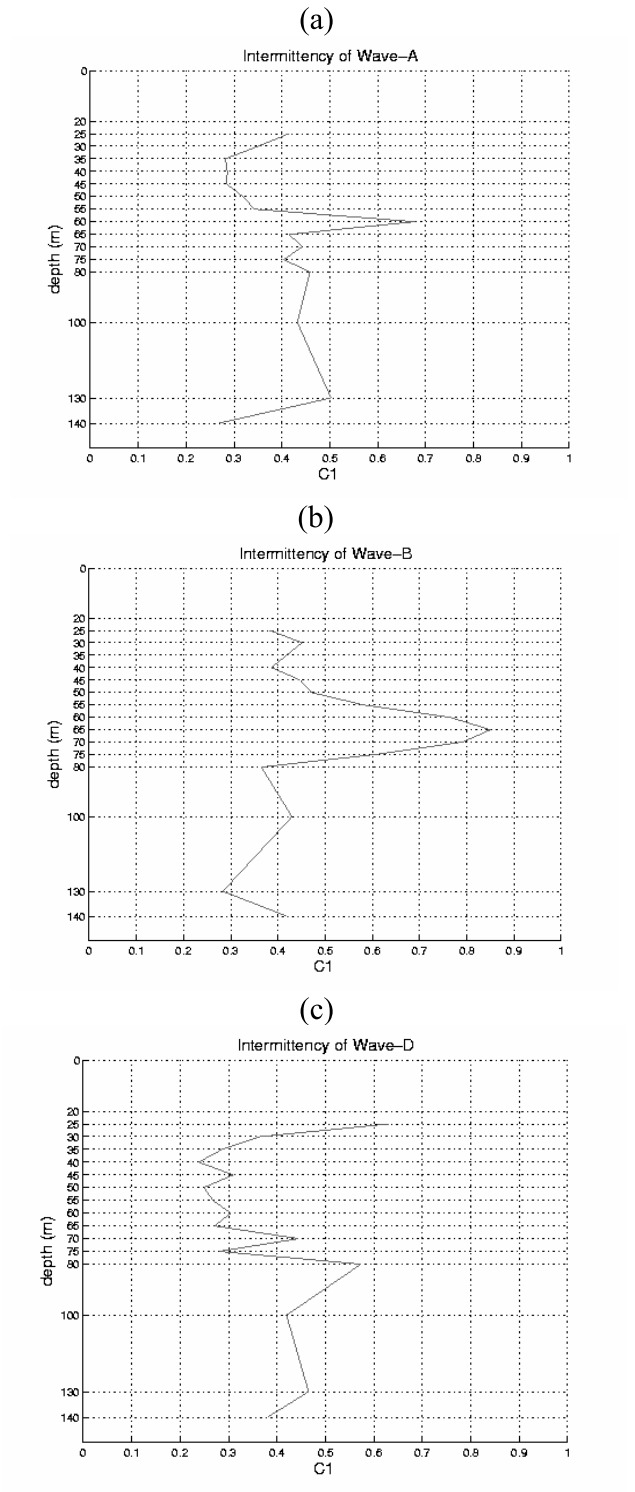

Fig. 14. Depth-dependent intermittency parameter C_1 on (a) 1000–1500 GMT July 29 (IW-turbulence), (b) 0700–1200 GMT July 30 (IS-turbulence), and (c) 0000–0500 GMT August 1 (turbulence-dominated), 2005.

$$C_1 \equiv C(1) = K'(1) \geq 0, \tag{23}$$

which is called the intermittency parameter. The larger the value of C_1, the larger the intermittency and singularity in the data set. The C_1-value is computed at all depths for the three types. The intermittency parameter C_1 varies from 0.25 to 0.6 for the turbulence-dominated type (Fig. 14(c)), from 0.25 to 0.67 for the IW-turbulence type (Fig. 14(a)), and 0.29 to 0.84 for the IS-turbulence type (Fig. 14(b)). The highest intermittency (maximum value of C_1) occurs at the upper-most part for the turbulence-dominated type, but at the mid-level for the IW-turbulence (60 m deep) and IS-turbulence (65 m deep) types. High C_1 values (>0.7) do not occur in the turbulence-dominated type and IW-turbulence type, but occur in the middle layer (58–73 m, where the thermocline is located, see Fig. 5(b)) in the IS-turbulence type, which indicates that the internal solitons generate high intermittency around the thermocline.

8. Explanation

One may ask: What causes the multifractal characteristics of the structural function break in the IS-turbulence with coherent structures? Why are the multifractal characteristics broken? Since the major task of this paper is to analyze the high-resolution temperature data, we only present a relatively simple explanation rather than a thorough mathematical derivation.

The total energy of the internal waves may be represented as an integral over spectral energy density,

$$E = \int E(\mathbf{k}, m) d\mathbf{k} dm, \tag{24}$$

where $\mathbf{k}$ and m are the horizontal components of the wave vector. Under the assumption of horizontal isotropy, Garrett and Munk proposed an empirical expression for the spectral energy density (Garrett and Munk, 1975). Using the Hamitonian formulation, Lvov and Tabak (2001) modified the Garrett-Munk spectrum into

$$E(k,m) = \frac{2fNE}{\pi} \frac{\left(m/m^*\right) A\left(m/m^*\right)}{N^2 k^2 + f^2 m^2},$$
$$m^* \equiv \gamma\left(\omega^2 - f^2\right)^{-\delta/2}, \quad A(\lambda) \equiv \frac{t-1}{(1+\lambda)^t}, \tag{25}$$

which represents both internal waves and wave turbulence. Here, E is a constant, quantifying the total energy content of the internal wave spectrum; f is the Coriolis parameter; ω is the wave frequency; N is the buoyancy frequency; $k = |\mathbf{k}|$, (t, δ, γ) are constants to be determined from observations. Similar multifractal characteristics of the structural function between IW-turbulence and turbulence-dominated types may be because the energy spectrum (25) represents internal waves and wave turbulence. However, the internal solitary waves are a class of nonsinusoidal, nonlinear, more-or-less isolated waves of complex shape that maintain their coherence. The internal solitons are usually composed of several oscillations confined to limited region of space, and their energy spectrum is totally different from the internal wave spectrum (25). This might be the reason for the multifractal characteristics of the structural function break at near half of the oscillation period (8 min) in the IS-turbulence with coherent structures. Numerical modeling is needed in the future to fully explain this phenomenon.

9. Conclusions

The temperature of the WPS upper layer (to 140 m deep) was sampled at high frequency from July 28 to August 7, 2005 using a coastal monitoring buoy with 15 attached thermistors. The isopycnal displacement is calculated from the temperature field, and the internal waves and solitons were observed.

(1) Three types of thermal variability are identified: IW-turbulence, IS-turbulence, and turbulence-dominated. The power spectra of temperature at all depths have multiscale characteristics. The IW-turbulence type has almost the same spectral exponents β as the turbulence-dominated type (two scales) with around 0.4 (stationary) for low wavenumbers and nearly 5/3 for high wavenumbers ($\log_2 kL/2 > 4$); but with much larger energy $E(k)$ than the turbulence-dominated type. This implies that the energy is distributed in all wavenumbers during the internal wave propagation. The spectrum for the IS-turbulence type is quite different from the two other spectra, especially in the spectral exponent β (three scales): around 0.4 for low wavenumbers, nearly 4.2 for mid-range wavenumbers, and approximately 5/3 for high wavenumbers.

(2) Without the internal waves and solitons (turbulence-dominated type), the temperature fluctuation has maximum values at the surface, decreases with depth to mid-depths (60–65 m deep), and then increases with depth to 140 m. Such a depth-dependent (decreasing then increasing) pattern is preserved during the internal wave propagation in the period 1000–1500 GMT July 29, 2005. However, this changed during the internal soliton propagation to a pattern that increases with depth from the surface to 60 m deep, decreases with depth from 60 m to 100 m deep, and increases again with depth from 100 m to 140 m. The temperature fluctuation enhances with the internal wave and soliton propagation. Between the two, the internal solitons introduce larger fluctuations.

(3) The observed temperature profile does not oscillate if there is no internal wave and soliton propagation. The oscillation is evident in the upper layer above

50 m with the internal wave propagation and above 80 m with the internal soliton propagation. The amplitude of the oscillation is much larger during the internal soliton propagation (maximum amplitude around 4°C) than the internal wave propagation (maximum amplitude around 2°C).

(4) The structure function satisfies the power law with multifractal characteristics for the IW-turbulence type and turbulence-dominated type, but not for the IS-turbulence type. The internal waves increase the power of the structure function, especially for high moments. The internal solitons destroy the multifractal characteristics of the structure function. The power law is broken approximately at a lag of 8 min, which is nearly one half period of the IS (with frequency of 4 CPH).

(5) The singular measure (representing the intermittency) satisfies the power law with multifractal characteristics for all the three types (IW-turbulence, IS-turbulence, and turbulence-dominated). The intermittency parameter C_1 does not change very much during the internal wave propagation, but increases drastically during the internal soliton propagation, which implies that the internal waves do not generate extra intermittency, but the internal solitons generate high intermittency.

(6) Multifractal analysis provides a useful framework for the analysis of ocean data when complex nonlinear processes exist. For the data collected from the CMB with attached thermistors, it clearly shows different effects on the upper ocean multifractal thermal structure between internal wave and internal soliton propagation. The physical mechanisms causing these different effects need to be explored further. Moreover, the universality of the multifractal properties obtained in this paper should be tested in different oceans and fluid phenomena, especially the breakdown of multifractal characteristics in the IS-turbulence type when coherent structures appear in turbulent fields.

Acknowledgements

This work was funded by the Office of Naval Research, Naval Oceanographic Office, and the Naval Postgraduate School.

References

Chu, P. C. (2004): Multifractal thermal characteristics of the southwestern GIN Sea upper layer. *Chaos, Solitons and Fractals*, **19**(2), 275–284.

Chu, P. C. and C. W. Fan (2001): Low salinity, cool-core cyclonic eddy detected northwest of Luzonduring the South China Sea Monsoon Experiment (SCSMEX) in July 1998. *J. Oceanogr.*, **57**, 549–563.

Chu, P. C. and C.-P. Hsieh (2007): Multifractal thermal characteristics of the western Philippine Sea upper layer. *Indian J. Mar. Sci.*, **36**(2), 141–151.

Chu, P. C. and R. F. Li (2000): South China Sea isopycnal surface circulation. *J. Phys. Oceanogr.*, **30**, 2419–2438.

Chu, P. C., L. Ivanov, L. Kantha, O. Melnichenko and Y. Poberezhny (2002): Power law decay in model predictability skill. *Geophys. Res. Lett.*, **29**(15), DOI:10.1029/2002GLO14891.

Desaubles, Y. and M. C. Gregg (1981): Reversible and irreversible finestructure. *J. Phys. Oceanogr.*, **11**, 541–556.

Garrett, C. J. R. and W. H. Munk (1975): Space-time scales of internal waves, a progress report. *J. Geophys. Res.*, **80**, 281–297.

Liu, A. K., Y. S. Chang, M.-K. Hsu and N. K. Liang (1998): Evolution of nonlinear internal waves in the East and South China Seas. *J. Geophys. Res.*, **103**, 7995–8008.

Lvov, Y. V. and E. G. Tabak (2001): Hamiltonian formalism and the Garrett-Munk spectrum of internal waves in the ocean. *Phys. Rev. Lett.*, **87**, 168501-1 to 168501-4, DOI:10.1103/PhysRevLett.87.168501.

Nitani, H. (1972): Beginning of Kuroshio. p. 129–163. In *Kuroshio: Its Physical Aspects*, ed. by H. Stommel and K. Yoshida, University of Tokyo Press, Tokyo.

Ramp, S. R., T.-Y. Tang, T. F. Duda, J. F. Lynch, A. K. Liu, C.-S. Chiu, F. L. Bahr, H.-R. Kim and Y.-J. Yang (2004): Internal solitons in the northeastern South China Sea Part I: Sources and deep water propagation. *IEEE J. Oceanic Eng.*, **29**, 1157–1180.